Electronic Supplementary Material (ESI) for Nanoscale.
This journal is © The Royal Society of Chemistry 2023

SUPPLEMENTARY INFORMATION on
Tuning the carrier injection barrier of hybrid metal-organic interfaces on rare earth-gold surface compounds

R. Castrillo-Bodero,[a], M. Blanco-Rey,[b,c], K. Ali,[a,c], J.E. Ortega,[d,a,c], F. Schiller,[a,c] and L. Fernandez*[a]

[a] *Centro de Física de Materiales CSIC/UPV-EHU-Materials Physics Center, 20018 San Sebastián, Spain.*
[b] *Universidad del País Vasco UPV-EHU, Dpto. de Polímeros y Materiales Avanzados: Física, Química y Tecnología, 20018 San Sebastián, Spain.*
[c] *Donostia International Physics Center, 20018 Donostia-San Sebastián, Spain.*
[d] *Universidad del País Vasco UPV-EHU, Dpto. Física Aplicada I, 20018 San Sebastián, Spain.*

The supplementary information file contains:
Supplementary Figures S1-S11.
Table S1.
Section S1: Molecular level renormalization with DFT.
Section S2: Physisorption and charge redistribution at metal-organic interfaces

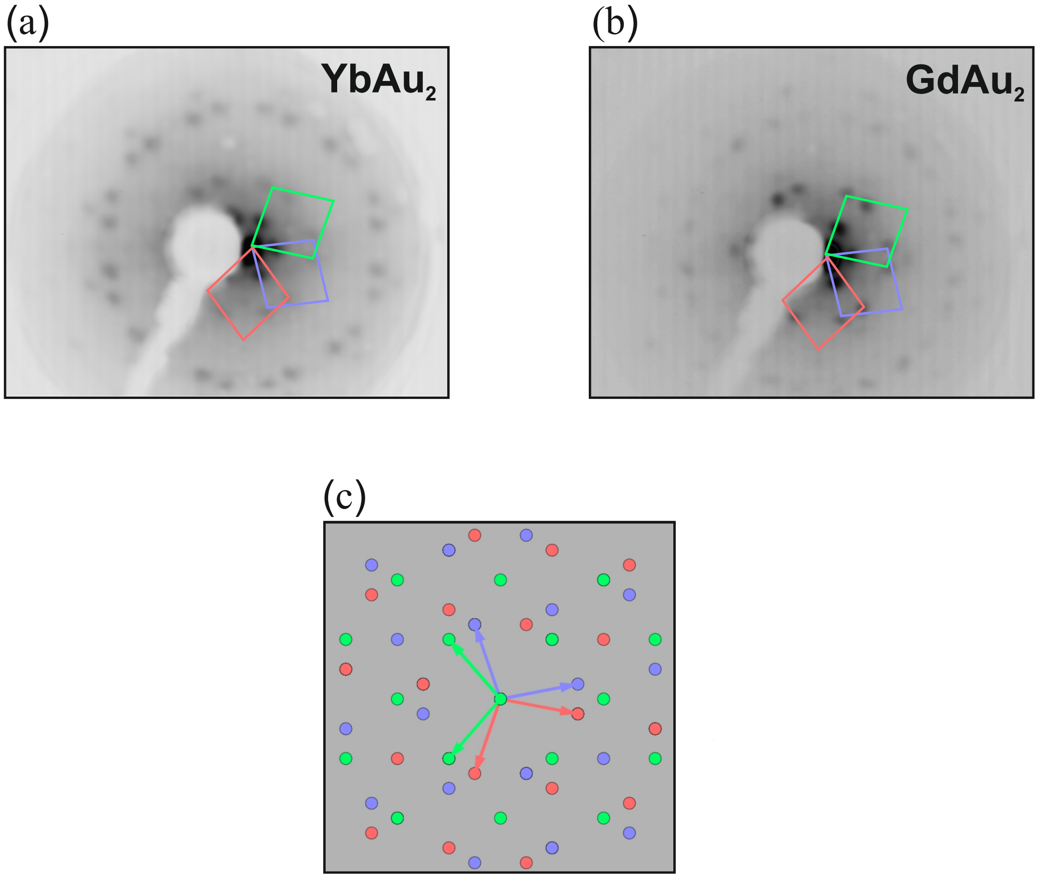

Figure S1 LEED patterns of the commensurate CuPc on (a) YbAu$_2$ and (b) GdAu$_2$ surfaces taken at 11.5 eV. The surface unit cells of the three equivalent rotational domains are displayed here (red, green and blue lines). All of them together contribute to the observed pattern. (c) Diffraction spots of each rotational domain are represented by a different color.

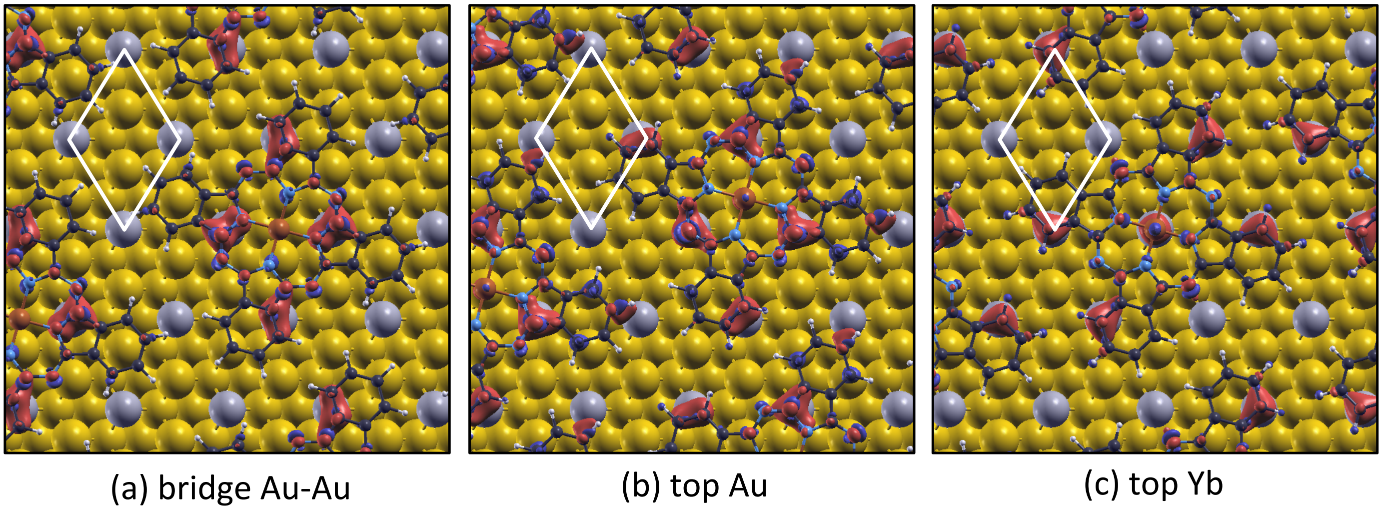

Figure S2 Calculated carrier density difference isosurface at $0.015\, n_e \text{Å}^{-3}$ for CuPc adsorbed at the three sites of YbAu_2/Au(111) 2 ML. The white line indicates the substrate unit cell. Note that the main charge rearrangement at the interface occurs above the Yb atomic positions (grey color). The bridge site between the Au atoms (golden color) introduces four such hotspots, while the two atop configurations give five. A similar result is found in the GdAu_2 case.

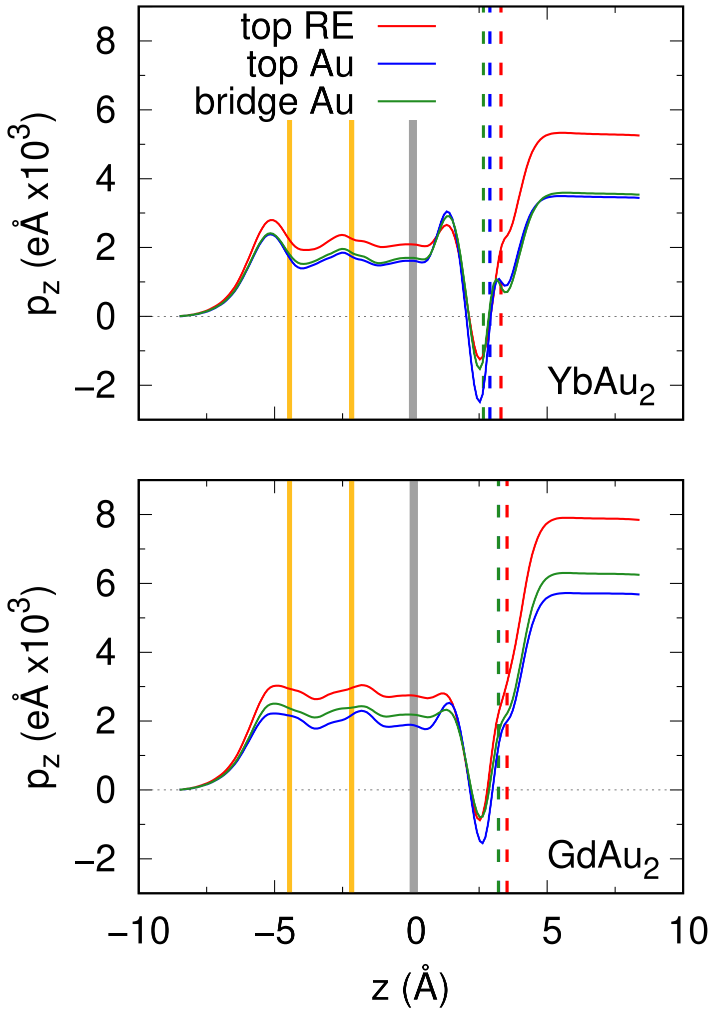

Figure S3 Plane-averaged accumulated dipole across the interface, calculated as $p_z(z) = -e\int_{z_1}^{z}\zeta\Delta\rho(\zeta)\mathrm{d}\zeta$, where $\Delta\rho(\zeta)$ is the plane-integrated charge density difference, for CuPc adsorbed at the CuPc/REAu$_2$/Au(111) 2 ML interfaces with RE=Yb and Gd. The vertical lines correspond to the atomic plane positions: Au (solid yellow), REAu$_2$ (solid gray), Cu atom (dashed, colors as *per* adsorption site). The plateau in the metallic slab region is due to the surface dipole at the Au(111) bilayer bottom. To obtain the p_z formed at the CuPc/REAu$_2$ interface, that slab bottom contribution to the integral is eliminated by taking z_1 at the middle point between the Au atomic planes. The resulting final values, which are dominated by the charge redistribution near the molecule plane, are shown in the main paper Table II.

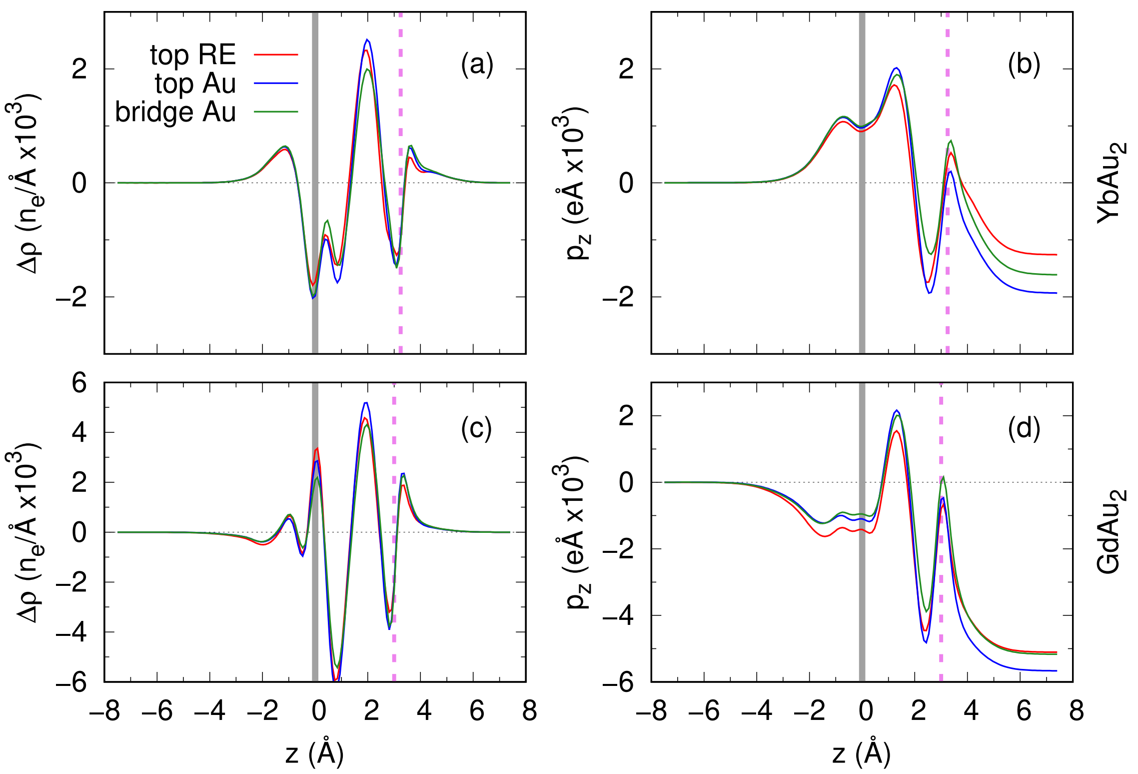

Figure S4 Plane-averaged carrier density difference $\Delta\rho(z)$ and accumulated dipole $p_z(z)$ for CuPc adsorbed at free-standing (a,b) YbAu$_2$ and (c,d) GdAu$_2$. The vertical lines correspond to the atomic plane positions: Au (solid yellow), REAu$_2$ (solid gray), and Cu atom (dashed purple). The curve colors indicate the adsorption site.

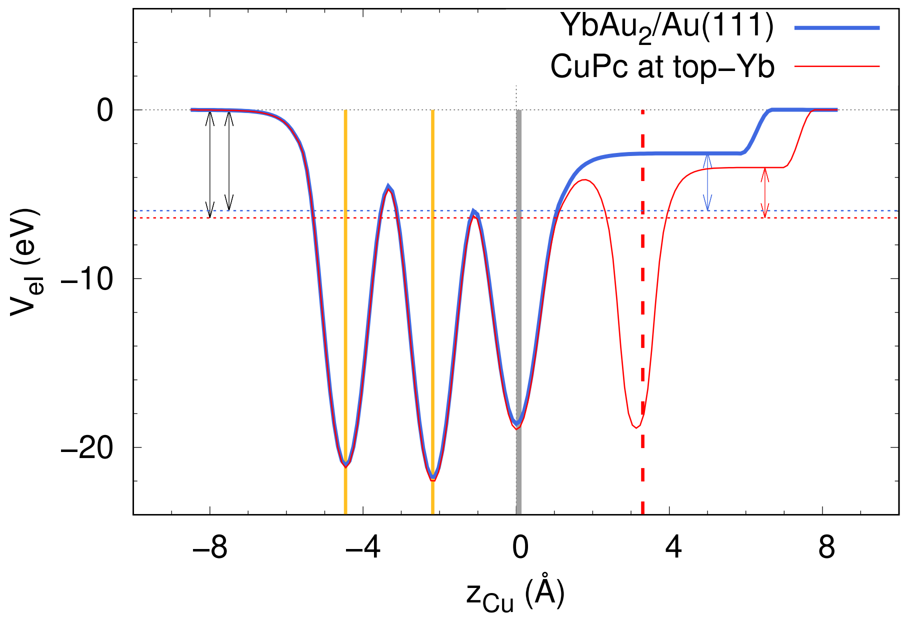

Figure S5 Plane-integrated electrostatic potential V_{el} calculated for the CuPc molecule adsorbed at the Yb site in YbAu$_2$/Au(111) 2 ML (red) and for the bare substrate (blue) plotted as a function of the supercell height. The jumps in V_{el} at 6-7 eV are due to the dipole correction in the calculation. The horizontal dashed lines are the Fermi levels in each case. The vertical lines indicate the Au planes (yellow solid), YbAu$_2$ plane (gray solid) and Cu atom height (red dashed). The Au(111) potential of the slab bottoms is taken as the zero energy reference. Both V_{el} curves have been aligned in this way. Because of finite slab thickness, the reference Au(111) work functions (black arrows on the left) are not equal. The difference between them can be considered to be an error bar for work functions of the CuPc/YbAu$_2$/Au(111) and YbAu$_2$/Au(111) surfaces (red and blue arrows, respectively, on the right).

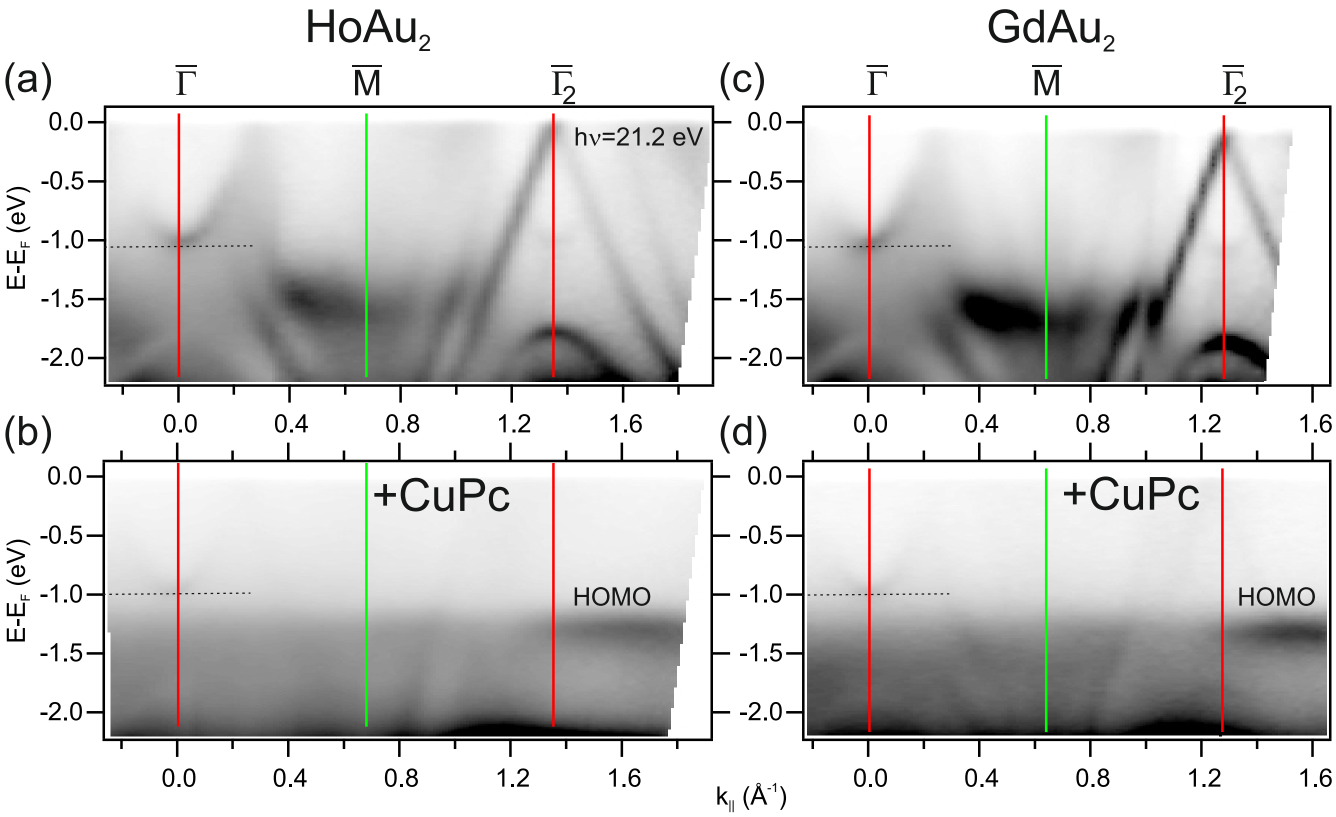

Figure S6 ARPES mapping intensity plots of (a) 1 ML of pristine $HoAu_2$, (b) 1 ML of CuPc on $HoAu_2$, (c) 1ML of pristine $GdAu_2$ and (d) 1 ML of CuPc on $GdAu_2$. The measurement direction corresponds to the $\bar{\Gamma}\bar{M}\bar{\Gamma}_2$ direction of the $\sqrt{(3)} \times \sqrt{(3)}$R30° surface Brillouin zone, hν = 21.2 eV. The HOMO of the adsorbed CuPc monolayers is also visible as a non-dispersing band.

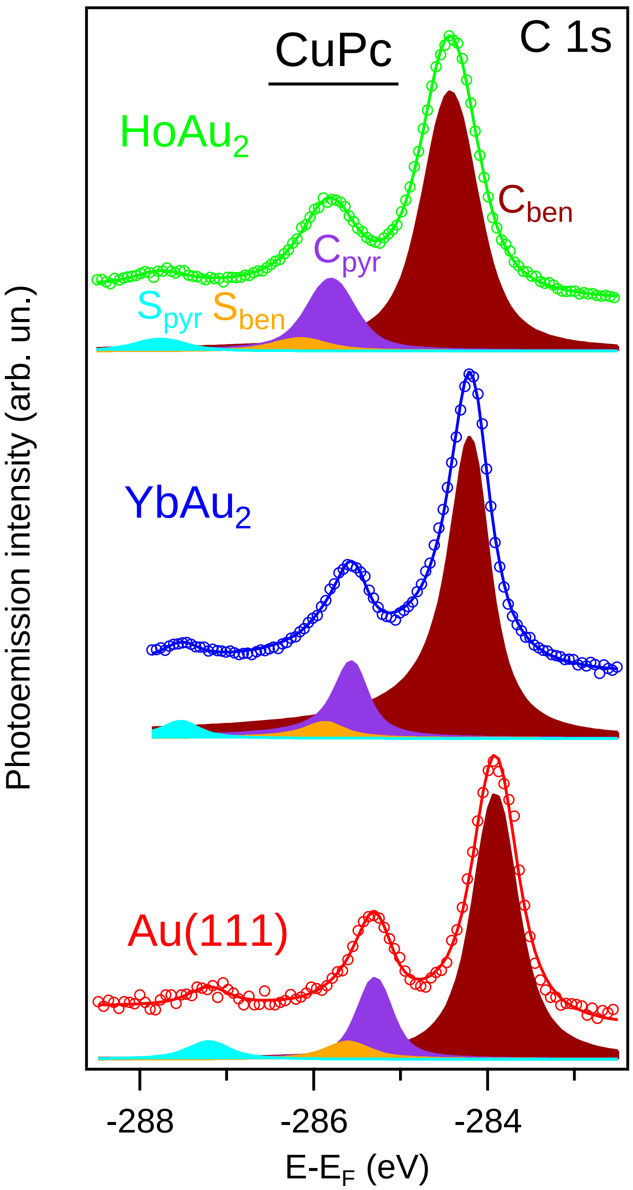

Figure S7 Peak fit analysis of the XPS C 1s core level emission of CuPc molecules on Au(111), YbAu$_2$, and HoAu$_2$. Data (circles) were taken with hν = 390 eV at the VUV Photoemission beamline of Elettra synchrotron in Trieste, Italy. For the fit (solid lines) four Doniach-Šunjic peaks[1] corresponding to the C-C (benzene-C_{ben}) and C-N (pyrrole-C_{pyr}) carbon atoms and their shake-up's (S_{ben}, S_{pyr}) were used as suggested in literature[2–5]. Furthermore, in the fit a Shirley background[6] was added to each peak. Due to the overlapping of the C-N and the C-C shake-up emissions, constraints were set. We constrained that all peak asymmetries and Shirley backgrounds were identical for all four peaks and the widths of the shake-ups were constrained to have the same width as the leading peak. The last constraint that was set is that the main peak/shake-up distances for C-C and C-N were identical. As a result of the fit, the width of C-C and C-N peaks (and it shake-ups as a consequence of the constrains) resulted quite similar (0.38±0.06) meV FWHM. The intensity relation of C-C:C-N was very close to 3:1 in all investigated cases. The most important difference between these three systems is the peak shift between each data set amounting to 0.26eV (CuPc/Au(111) to CuPc/YbAu$_2$) and 0.49eV (CuPc/Au(111) to CuPc/HoAu$_2$) with the leading C-C peak positions at 283.94eV, 284.18eV, and 284.42eV, respectively, for CuPc on Au(111), YbAu$_2$, and HoAu$_2$.

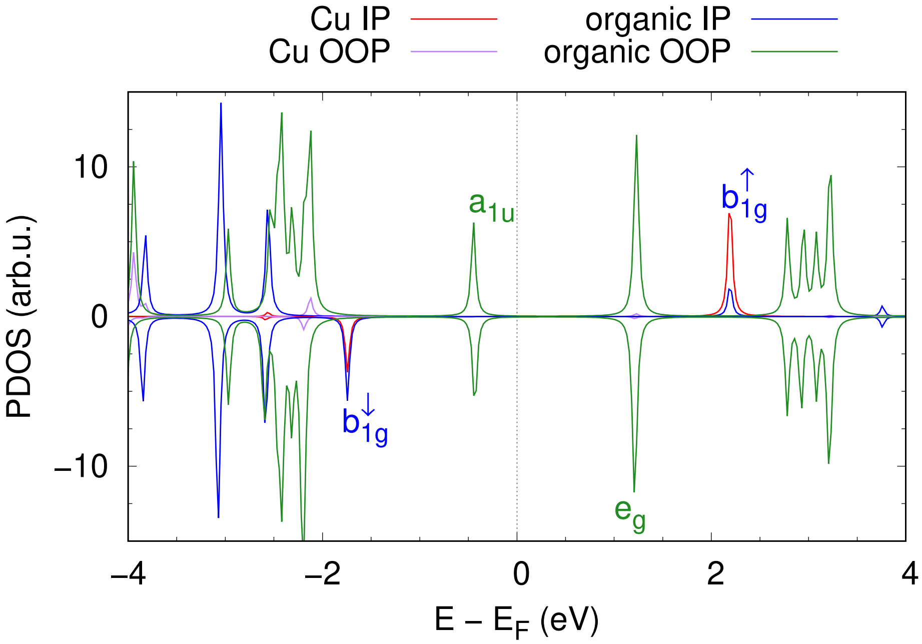

Figure S8 HSE03 functional calculation of the projected density of states (PDOS) on atomic orbital groups of the isolated CuPc molecule. The Cu in p-plane (IP) orbitals are $d_{x^2-y^2}, d_{xy}$; Cu out-of-plane (OOP) are d_{xz}, d_{yz}, d_{z^2}; organic IP are p_x, p_y of C and N; and organic OOP are p_z of C and N.

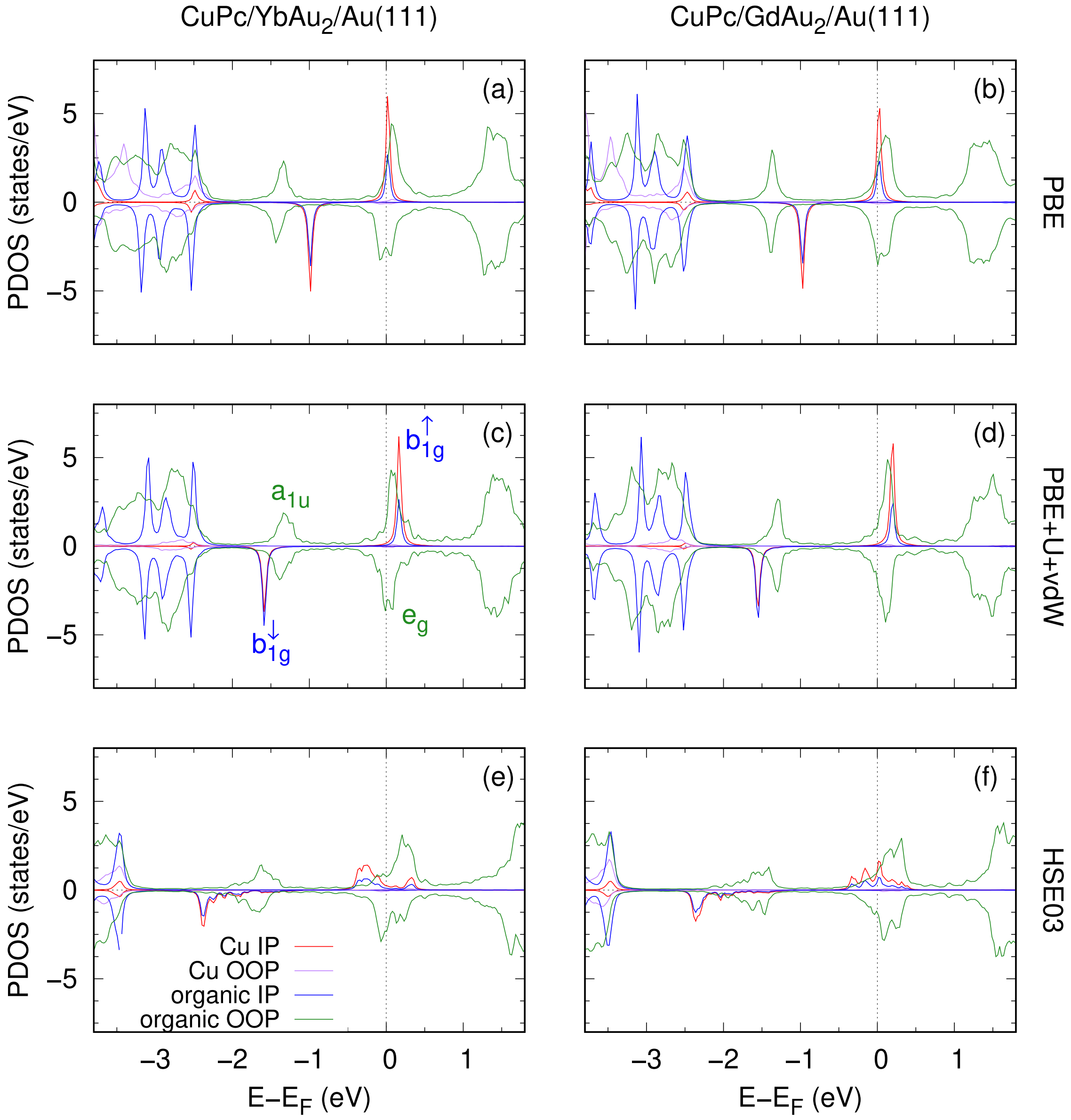

Figure S9 PDOS projected on atomic orbital groups of CuPc in CuPc/REAu$_2$/Au(111), which account for relevant CuPc frontier molecular orbitals, obtained with (a,b) PBE, (c,d) PBE+U+vdW and (e,f) HSE03 exchange and correlation functionals. Left and right columns are for RE=Yb and Gd, respectively. Spin majority and minority states correspond to positive and negative PDOS values, respectively. The Cu in-plane (IP) orbitals are $d_{x^2-y^2}, d_{xy}$; Cu out-of-plane (OOP) are d_{xz}, d_{yz}, d_{z^2}; organic IP are p_x, p_y of C and N; and organic OOP are p_z of C and N. Note, the HSE03 PDOS is obtained in a perturbative approximation by applying the exact Hartree-Fock contribution non-selfconsistently to PBE wavefunctions.

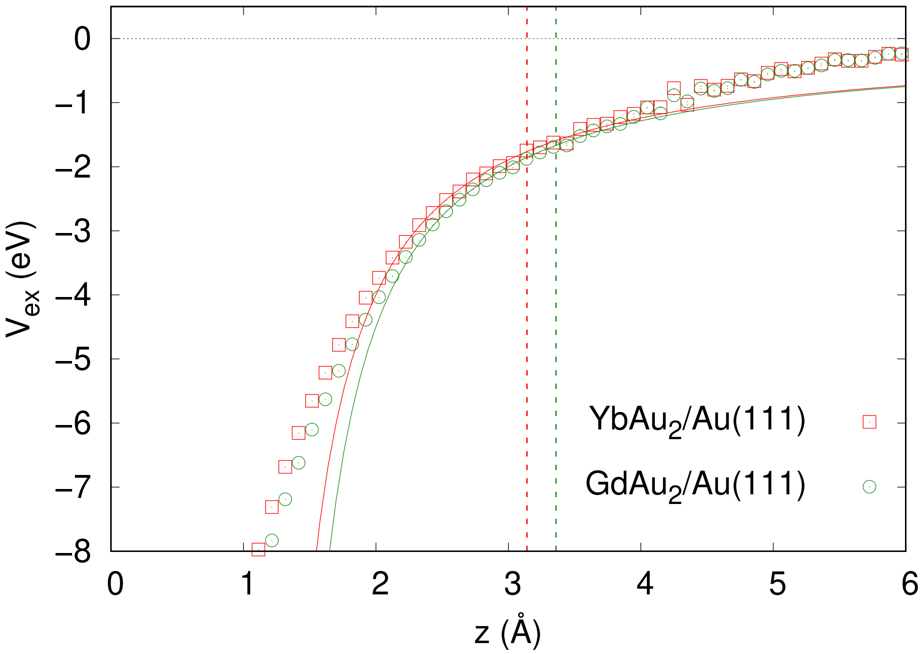

Figure S10 PBE calculation of the plane-averaged exchange correlation potentials for the $REAu_2$ on a Au(111) bilayer (RE=Yb,Gd) to be used in the DFT+Σ_{axc} approach. The solid curves are the image potentials of expression $-\frac{1}{4(z_{\text{HOMO}}-z_0)}$, where the z_0 parameter is fit by matching with the PBE data points at the point of common curvature.

Table S1 Geometry details for CuPc adsorbed at RE atop positions of $REAu_2$/Au(111), as obtained in DFT+U+vdW calculations. The average of C and N atom heights is taken as the HOMO height used in the DFT+Σ_{axc} determination of HOMO levels, as explained in section S1. The substrate image potential parameters z_0 have been extracted from the curves shown in Fig. S10. The values in parenthesis indicate the root mean square deviation.

	$YbAu_2$/Au(111)	$GdAu_2$/Au(111)
z_{Cu} (Å)	3.31	3.53
$z_{\text{HOMO}} = \langle z_{\text{C,N}} \rangle$ (Å)	3.14 (0.08)	3.36 (0.09)
z_0 (Å)	1.1	1.2
$\varepsilon_{\text{HOMO}}^{\text{DFT}+\Sigma_{\text{axc}}}$ (eV)	-0.92	-1.02

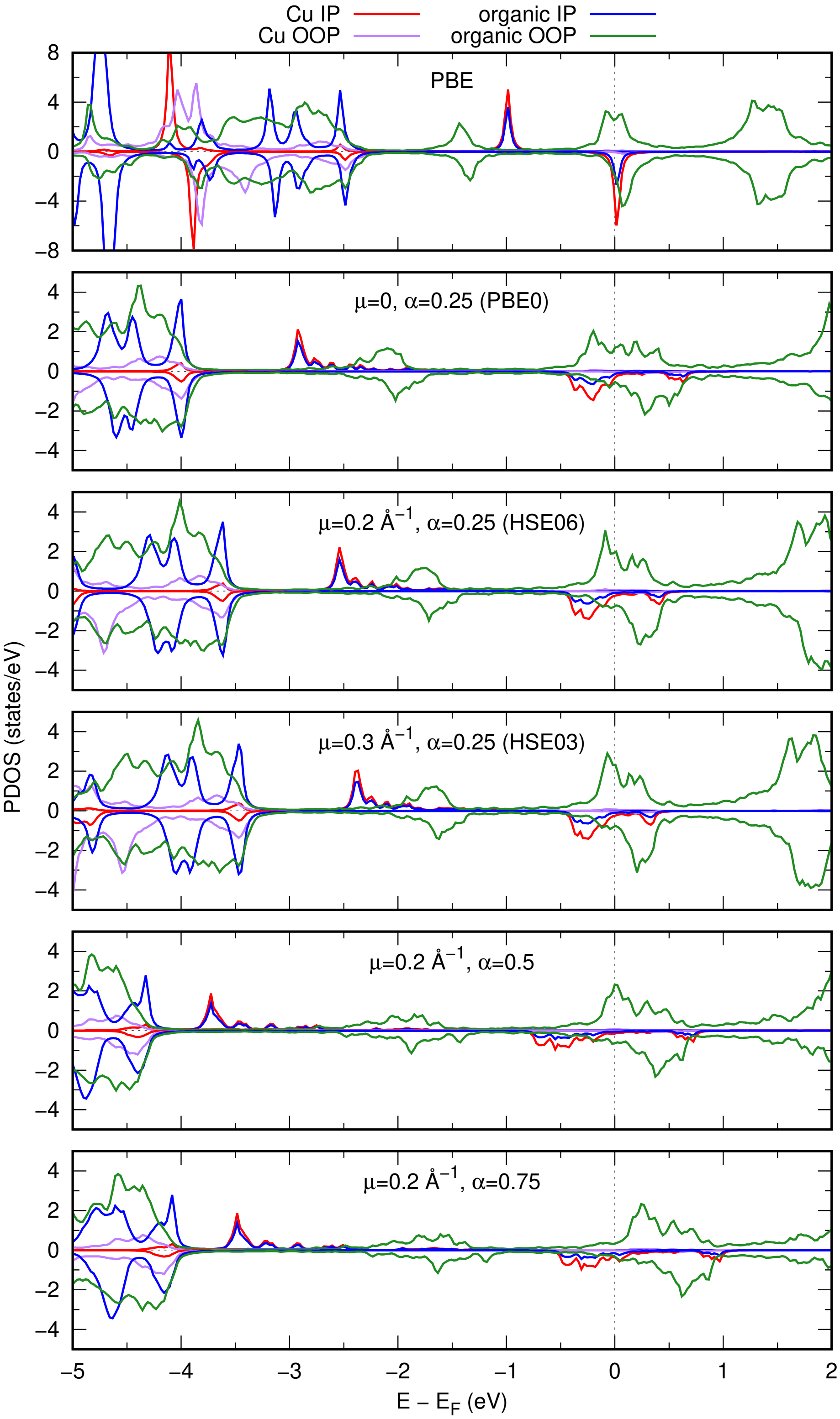

Figure S11 Survey of hybrid functionals for CuPc/YbAu$_2$/Au(111) (adsorption at Yb-top). For each pair of screening range μ and exact exchange fraction α parameters, the PDOS is calculated perturbatively, i.e. the exact Hartree-Fock contribution is applied non-selfconsistently to wavefunctions of the PBE calculation (top panel) and new eigenenergies are obtained. Therefore, the resulting peaks are broad. Note, the LUMO pinning at Fermi persists, as the reference peak in PBE is more than half-occupied. Same color code as Fig. S8.

S1 Molecular level renormalization with DFT

Some features in the projected densities of states (PDOS) on the molecular orbitals calculated by DFT+U+vdW (see Fig. S9(c,d)) are not consistent with the experimental observations. Here, broadening and pinning at the Fermi level of the LUMO (of e_g symmetry) are observed, but the absence of photoemission signatures of this pinning effect suggests that it might be an artifact due to self-interaction errors (SIE) [7] in the DFT approach. Besides, the positions of the CuPc HOMO levels (a_{1u}) on both substrates, at around $E_F - 1.45$ eV, are considerably downshifted with respect to the experimental ones. We conclude that the DFT+U+vdW approach is insufficient to correctly describe the alignment of molecular orbital levels with respect to the substrate electronic states. When compared with PBE calculations (see Fig. S9(a,b)), the DFT+U+vdW calculation corrects the PBE description of the singly-occupied molecular orbital (SOMO, b_{1g}). Indeed, DFT+U+vdW correctly places the SOMO below the a_{1u} level[8–11], leaving a clearly unoccupied half. However, the LUMO level pinning at the Fermi level persists.

Contrary to Hartree-Fock (HF) approach, in DFT there is not an exact cancellation of the electron self-interaction in the Coulomb and exchange parts of the energy functional[7]. In our case, the SIE is manifested as an overestimated HOMO binding energy and a pinning of the LUMO at Fermi. The theoretical challenge posed by the SIE has been tackled with the use of hybrid functionals, which contain a fraction α of exact exchange within a given range $2/\mu$. These two parameters define the functional flavour. Fig. S9(e,f) show the PDOS obtained with the HSE03 hybrid functional[12] ($\alpha = 0.2$, $\mu = 0.3$ Å). However, many-body effects such as polarizability of the substrate, are missing from the DFT description even with exact exchange[13,14], which can affect specifically the orbital alignment with neighbouring metal states. Here, GW computational methods[15] for metal/organic interface problems become prohibitively expensive. To circumvent these issues, we resort to the DFT+Σ_{axc} method for the occupied orbitals[16] in order to determine the HOMO level alignment in CuPc/REAu$_2$/Au(111). This method consists in renormalizing the reference PBE level with the correction to the CuPc gas-phase HOMO level (HOMO(g)) with the asymptotic form of the substrate exchange-correlation potential (an image potential) at the HOMO position. The resulting equation for the corrected eigenvalues is:

$$\varepsilon_{\text{HOMO}}^{\text{DFT}+\Sigma_{\text{axc}}} = \varepsilon_{\text{HOMO}}^{\text{PBE}} + (\varepsilon_{\text{HOMO(g)}}^{\text{OT-RSH}} - \varepsilon_{\text{HOMO(g)}}^{\text{PBE}}) + \frac{1}{4(z_{\text{HOMO}} - z_0)}.$$

Here, the first term is the HOMO level provided by a PBE calculation. The second term is the HOMO(g) correction to the PBE value with the optimally tuned range-separated hybrid (OT-RSH) functional[17], known to provide frontier orbital energies in some organic and organometallic molecules with comparable accuracy to GW methods[18]. For this term we use the value -1.3 eV reported in Ref.[10]. Finally, the third term in Eq. 1 is the Coulomb long-distance potential decay with distance z from the bare REAu$_2$/Au(111) 2 ML substrates, where the z_0 parameter is obtained by matching the derivative of the analytical image potential expression with that of the calculated plane-averaged PBE exchange and correlation potential V_{xc},[10] (this means that the V_{xc} corrugation in (x, y) is neglected in the model). This interaction term is evaluated at the height of the CuPc HOMO, z_{HOMO}. Since the adsorbed molecule is slightly buckled in the optimized geometry, we do not use the Cu atom height to evaluate the interaction term for the HOMO. Instead, for z_{HOMO} we use the average height of the C and N atoms only where the HOMO (a_{1u}) is localized.

The calculated plane-averaged $V_{xc}(z)$ potentials for both substrates, which behave as the usual image potential of a metallic surface, are given in Fig. S10. The resulting energies, as well as the used geometry parameters, are shown in Table S1. Note that the DFT+Σ_{axc} approach is highly dependent on geometry details and, therefore, several approximations need to be made that involve taking averaged geometry parameters (see Methods). All in all, the result shows the same trend as the experiment, namely, the CuPc HOMO on YbAu$_2$ lies $\simeq 0.1$ eV closer to the Fermi level than on GdAu$_2$, but the actual binding energies differ by $\simeq 0.2$ eV.

The HOMO-LUMO gap is usually reduced in the adsorbed configuration by renormalization and this reduction correlates with the static response function, thus with the metallic substrate density of states at the Fermi level[14]. With the HSE03 functional we determine a gap for the isolated CuPc layer of 2.15 eV (see Fig. S8). This is close to the literature value of the isolated molecule with this functional, 1.8 eV[8], which shows that the lateral interaction between molecules does not significantly affect the gap. In the DFT+U+vdW approach, the gap value in the adsorbed configurations is reduced to 1.35 and 1.42 eV in the adsorbed configurations at the Yb and Gd sites, respectively (see Fig. S9(c,d)). In calculations with the HSE03 hybrid functional for the same geometry, the gap is similar and the LUMO remains pinned at Fermi level (see Fig. S9(e,f)). With the same level of theory, comparable gap sizes and absence of Fermi level pinning have been reported for CuPc on Au(111) and Au(110)[19,20], suggesting the pinning of Fig. S9 is unphysical and can be the consequence of several limitations in the functionals. First, the used vdW functional provides a geometry, in particular an adsorption height, which may correspond to a regime where the system would lie in the $V_{ads}(z)$ repulsive regime for the hybrid functional. This destabilization may manifest itself as a partial charging of the LUMO. For example, in CuPc/Au(110) interaction is stronger than in CuPc/Au(100), prompting a tilt of the molecule and a downshift of the LUMO to just a few cents of eV above Fermi[20]. Second, as shown in Ref.[21], a tuning of the hybrid functional parameter α can eventually (de)populate molecular adsorbate orbitals, but this will only happen, as a general rule, if it was less than half occupied in the PBE reference calculation. This is not our case for the e_g orbital at one spin polarity (see Fig. S9(a,b)). A survey of hybrid functionals shows that the pinning persists for different $2/\mu$ and α choices, sometimes with an inversion of the e_g and b_{1g} levels (see Fig. S11).

S2 Physisorption and charge redistribution at metal-organic interfaces

In the classic view, the semiconductor/metal contact leads to a Fermi level (E_F) repositioning inside the semiconductor gap. E_F gets fixed at the so-called charge neutrality level of the metal-induced gap states. If the interaction is weak (physisorption, push-back effect), these states may simply be viewed as the metal wave functions tailing inside the semiconductor gap. Every interface has its own charge neutrality level. If we change the metal, we just change the position of the charge neutrality level, that is, the position of the Fermi level inside the semiconductor (molecule) gap. Therefore, if we compare spectra from two different interfaces, we see a rigid shift of the whole spectrum. Any deviation from rigidity when comparing two interfaces should be ascribed to real metal/molecule local atomic bonding happening at a particular interface. This situation will lead to chemical shifts for the individual atoms involved, such that the spacing between energy levels is not preserved. However, in the here described interfaces of CuPc on $REAu_2$ such chemical shifts were not observed. On the other hand, a spatial redistribution of charge may not mean "bonding", it could in fact reflect the push-back effect in the real space. This means that, despite the spatial redistribution of the charge that we see in the studied systems, the rigidity strongly suggests that there is no significant molecule/surface interaction (bidirectional charge transfer or bonding) at these interfaces.

Furthermore, a Bader analysis[22,23] of the charges associated to each atom in the structure shows that the CuPc acquires 0.58 e^- when adsorbed at top-Yb in the PBE+U approach (the same as in Fig.3 of the main paper). However, we have reasons to believe that this is an artifact. We have shown that calculations in these systems at the DFT level are affected by the "self-interaction error" (SIE), which is manifested as a pinning of e_g molecular orbitals at the Fermi energy (see the PDOS in Fig. 6 of the main paper). This means that the SIE is highly inhomogeneous in $CuPc/REAu_2$ systems, a qualitatively different scenario to that of CuPc physisorbed on pure noble metals. Indeed, a breakdown of the Bader charges shows that most of the aforementioned 0.58 e^- are contributed by a few C atoms of the benzene rings. The robust experimental evidence, however, supports the absence of net charge transfer and, therefore, allows us to conclude that the Pauli pushback effect dominates. The theory at the DFT level cannot fully capture this complex many-body effect. Overall, pushback is underestimated and this is manifested in the PDOS as a Fermi pinning of a molecular orbital, with the associated electron transfer. As technical note, it can be commented that 0.58 e^- is an upper bound in the current systems. The case for Cu of the CuPc molecule at Yb top position has been chosen for this discussion because it appears to have the largest e_g peak at the Fermi level in the PDOS graphs. We remind, in passing, that charge-to-atom assignation methods are always subject to some arbitrariness, so that slightly different values may be obtained by techniques other than Bader's "atoms in molecules" approach, especially in a situation with a neighboring metal surface.

Notes and references

[1] S. Doniach and M. Šunjic, *Journal of Physics C: Solid State Physics*, 1970, **3**, 285.

[2] L. Ottaviano, S. Di Nardo, L. Lozzi, M. Passacantando, P. Picozzi and S. Santucci, *Surface Science*, 1997, **373**, 318–332.

[3] H. Peisert, M. Knupfer and J. Fink, *Surface Science*, 2002, **515**, 491–498.

[4] T. Schwieger, H. Peisert, M. S. Golden, M. Knupfer and J. Fink, *Phys. Rev. B*, 2002, **66**, 155207.

[5] B. Brena, Y. Luo, M. Nyberg, S. Carniato, K. Nilson, Y. Alfredsson, J. Åhlund, N. Mårtensson, H. Siegbahn and C. Puglia, *Phys. Rev. B*, 2004, **70**, 195214.

[6] D. A. Shirley, *Phys. Rev. B*, 1972, **5**, 4709–4714.

[7] J. P. Perdew and A. Zunger, *Phys. Rev. B*, 1981, **23**, 5048–5079.

[8] N. Marom, O. Hod, G. E. Scuseria and L. Kronik, *The Journal of Chemical Physics*, 2008, **128**, 164107.

[9] N. Marom, X. Ren, J. E. Moussa, J. R. Chelikowsky and L. Kronik, *Phys. Rev. B*, 2011, **84**, 195143.

[10] D. A. Egger, S. Weissman, S. Refaely-Abramson, S. Sharifzadeh, M. Dauth, R. Baer, S. Kümmel, J. B. Neaton, E. Zojer and L. Kronik, *Journal of Chemical Theory and Computation*, 2014, **10**, 1934–1952.

[11] Q. Zhou, Z.-F. Liu, T. J. Marks and P. Darancet, *The Journal of Physical Chemistry A*, 2021, **125**, 4055–4061.

[12] J. Heyd, G. E. Scuseria and M. Ernzerhof, *The Journal of Chemical Physics*, 2003, **118**, 8207–8215.

[13] J. B. Neaton, M. S. Hybertsen and S. G. Louie, *Phys. Rev. Lett.*, 2006, **97**, 216405.

[14] K. S. Thygesen and A. Rubio, *Phys. Rev. Lett.*, 2009, **102**, 046802.

[15] L. Hedin, *Phys. Rev.*, 1965, **139**, A796–A823.

[16] D. A. Egger, Z.-F. Liu, J. B. Neaton and L. Kronik, *Nano Letters*, 2015, **15**, 2448–2455.

[17] L. Kronik, T. Stein, S. Refaely-Abramson and R. Baer, *Journal of Chemical Theory and Computation*, 2012, **8**, 1515–1531.

[18] S. Refaely-Abramson, S. Sharifzadeh, N. Govind, J. Autschbach, J. B. Neaton, R. Baer and L. Kronik, *Phys. Rev. Lett.*, 2012, **109**, 226405.

[19] Y. L. Huang, E. Wruss, D. A. Egger, S. Kera, N. Ueno, W. A. Saidi, T. Bucko, A. T. Wee and E. Zojer, *Molecules*, 2014, **19**, 2969–2992.

[20] D. Lüftner, M. Milko, S. Huppmann, M. Scholz, N. Ngyuen, M. Wießner, A. Schöll, F. Reinert and P. Puschnig, *Journal of Electron Spectroscopy and Related Phenomena*, 2014, **195**, 293–300.

[21] O. T. Hofmann, V. Atalla, N. Moll, P. Rinke and M. Scheffler, *New Journal of Physics*, 2013, **15**, 123028.

[22] R. F. W. Bader, *Atoms in Molecules: A Quantum Theory*, Clarendon Press, 1994.

[23] G. Henkelman, A. Arnaldsson and H. Jónsson, *Computational Materials Science*, 2006, **36**, 354–360.